

High resolution THz scanning for optimization of dielectric layer opening process on doped Si surfaces

P. Spinelli¹, F.J.K. Danzl¹, D. Deligiannis^{1,2}, N. Guillevin¹, A.R. Burgers¹, S. Sawallich³,
M. Nagel³, I. Cesar¹

¹Energy Research Centre of the Netherlands (ECN), Petten, 1755 LE, The Netherlands

²Delft University of Technology, Delft, 2628 CD, The Netherlands

³Protemics GmbH, Aachen, 52074, Germany

Abstract — Diffused IBC solar cells based on non-fire-through (NFT) metallization can achieve higher performance with respect to FT metallization, thanks to lower contact resistance. Less resistive contacts allow for lower metal fraction and thus lower contact recombination. For the application of NFT contacts, the rear side dielectric passivation layer needs to be locally opened. Standard processes for dielectric opening include laser ablation, use of etching pastes or masking and etching. In all these cases it is important that the opening process does not cause any damage to the diffusion below the contacts. We present a fast inspection method based on THz near-field scanning that allows investigating the diffusion layers after dielectric opening with spatial resolution suited for the small feature size of standard IBC solar cells. This method can be used to optimize crucial parameters of the dielectric opening without processing full cells. In this paper, we use THz scanning to optimize the curing temperature of the etch paste used to open the dielectric passivation layers on solar cells half-fabricates. After optimization, full cells are processed with top efficiency of 20.8%.

I. INTRODUCTION

ECN “Mercury” cells are a bifacial IBC solar cell with a front floating emitter. The cells are processed at the cost level of PERC cells and can be easily interconnected into solar modules by, e.g., our conductive back-sheet foil technology [1]. The Mercury IBC cells have reached efficiencies up to 21.1%. [2] This result was achieved using a screen printed firing through (FT) metallization which is the current industry standard. The challenge of FT metallization is to limit the contact recombination as the frit fraction in the paste etches into the diffusion during firing for a significant depth. [3]. The emitter profile plays an important role in determining both the $j_{0,\text{contact}}$ and contact resistance of the FT metal contacts. [3]. Typical values of $j_{0,\text{contact}}$ for the FT metal contact range between 1000 fA/cm^2 and 2500 fA/cm^2 , as obtained by measuring specific test structures. [2] The high $j_{0,\text{contact}}$ of the emitter contact can thus cause significant open circuit voltage (V_{oc}) losses.

One way to reduce contact recombination is to use a non-fire-through (NFT) paste which can be applied also by screen

printing but does not require a high temperature firing step. As for the case of FT paste, the emitter profile plays an important role also for the NFT paste. Having a highly doped emitter in the surface region below the contact allows for better shielding of minority carriers and thus lower contact recombination. Concomitantly, the contact resistance of the metal paste is also strongly dependent on the surface dopant concentration. Hence, a non-etching paste has also the potential to have a lower contact resistance allowing lower contact areas or lighter surface dopants with lower surface recombination properties on the passivated areas of the solar cell.

The NFT metallization for the rear side of bifacial IBC solar cells needs to be applied in combination with a dielectric passivation layer for areas with no metallization. At ECN we use an $\text{Al}_2\text{O}_3/\text{SiN}_x$ dielectric stack to passivate the rear side surface of the Mercury cell. In order to apply the NFT metallization the dielectric layer stack needs to be locally opened. This can be done by several methods, such as by masking and chemical etching, laser ablation of the dielectric, or application of an etching paste. In order to achieve high efficiency IBC solar cells, the dielectric needs to be opened without damaging the diffusion below.

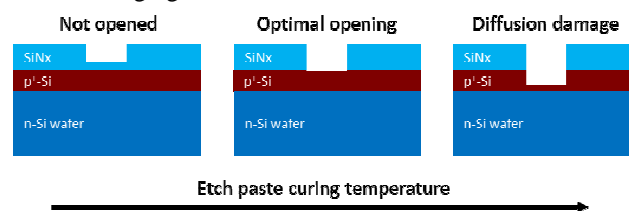


Fig 1. Schematic of three cases for the dielectric opening process.

Figure 1 shows schematics of three cases that can happen in the dielectric opening process. The optimal opening process is shown in the center panel. Under-etching (left panel) will result in poor or no contacting of the solar cell due to the residual dielectric layer in the opened area. On the other hand, over-etching (right panel) results in damaged diffusion layer under the contacts.

In this paper, we use THz near-field transmission scanning to investigate the homogeneity of the diffusions after opening of the dielectric. This method allows the optimization of any parameter which is crucial to any opening process (laser ablation, chemical etching, etc.) without the need to process full cells, and thus at a lower cost.

First, the THz transmission setup and R_{sheet} determination method are described, together with an analysis of the accuracy of the measurement for different feature sizes. Next, we consider the example of opening a SiN_x dielectric layer with an etching paste. We study the effects of the paste curing temperatures on the dielectric opening, in order to achieve an optimal opening process which does not damage the diffusion below the contacts. We demonstrate that the THz scanning method is not influenced by the surface morphology of the dielectric layer, but only by the diffusion below it. A full optimization of the dielectric opening process is shown at cell level.

II. THZ SHEET RESISTANCE MAPPING

A. THz transmission setup and R_{sh} determination

Sheet resistance (R_{sheet}) mapping is of great importance to characterize the homogeneity and doping levels of doped regions in solar cells. Usually 4-point probe (4pp) measurements are used to measure R_{sheet} . However, this method lacks the resolution required for a detailed inspection of IBC cells with sub-millimeter features.

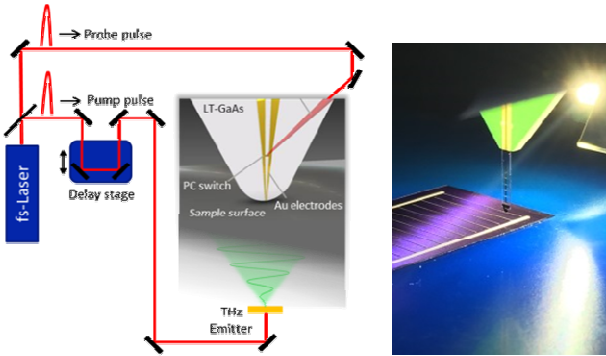


Fig 2. Schematic of the THz scanning setup (left) and photograph of the near field THz microprobe (right)

THz transmission near-field imaging is a method for high-resolution large-area sheet resistance quantification [4]. Such measurements uniquely allow monitoring the homogeneity of diffused layers with very high resolution enabling detection of features down to $20 \mu\text{m}$ in size. Measurements are performed in a THz transmission setup based on a pump/probe scheme, using broadband THz pulses. Figure 2a shows a schematic of the setup. Sub-wavelength spatial resolution is achieved by using a near-field microprobe (TeraSpike TD-800-X-HR, Protemics GmbH) for photo-conductive THz detection which

is scanned across the investigated IBC cell in a distance of few tens of microns (see photograph in Fig. 2b).

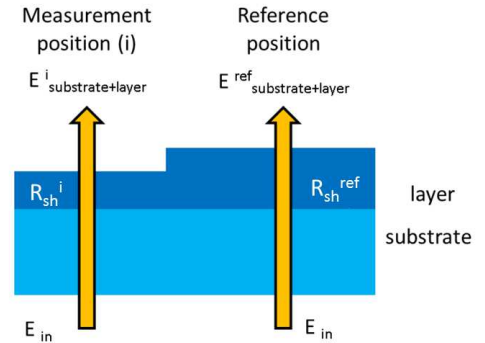


Fig 3. R_{sheet} maps of thin conductive layers are obtained from THz transmission maps by means of the Tinkham formula and a reference region with known R_{sheet} .

The sheet resistance (R_{sheet}) of a thin conductive layer on top of a substrate is calculated from the measured THz transmission amplitude reduction generated by the doping layer using the Tinkham formula [4]:

$$\frac{1}{R_{sh}^i} = \frac{n+1}{Z_0} \left[\frac{E_{SL}^{ref}}{E_{SL}^i} \left(1 + \frac{Z_0}{R_{sh}^{ref}(n+1)} \right) - 1 \right]$$

where E_{SL} represents the transmitted THz field amplitude through the sample with conductive layer, the superscript i indicates a position $i(x,z)$ anywhere on the sample, while the superscript ref indicates a position on a reference area on the sample with known R_{sheet} . Further constants are the substrate refractive index n and the free-space impedance Z_0 . The method can also take into account a second conductive layer on the other side of the cell (e.g. an FFE) if either the sheet resistance of this layer or its behavior in respect to the rear R_{sh} is known.

The THz transmission method allows fast (5 ms/pixel) and contact less R_{sheet} mapping in a range of 0.5Ω to $5 \text{ K}\Omega$ on substrates with typical background-doping levels ($<10^{16} \text{ cm}^{-3}$).

B. R_{sheet} accuracy and feature size

For quantitative analysis or doping patterns relevant for IBC solar cells, it is important that R_{sheet} can be accurately determined for feature sizes down to few tens of microns. We have investigated the accuracy of the R_{sheet} determination with THz scanning by means of test structures with features of known size and conductivity, obtained by evaporation and lift-off of thin Cr layers. By controlling the thickness of the metal layers, different values of R_{sheet} can be obtained. The test structures present feature sizes from 2.7 mm down to 10 microns.

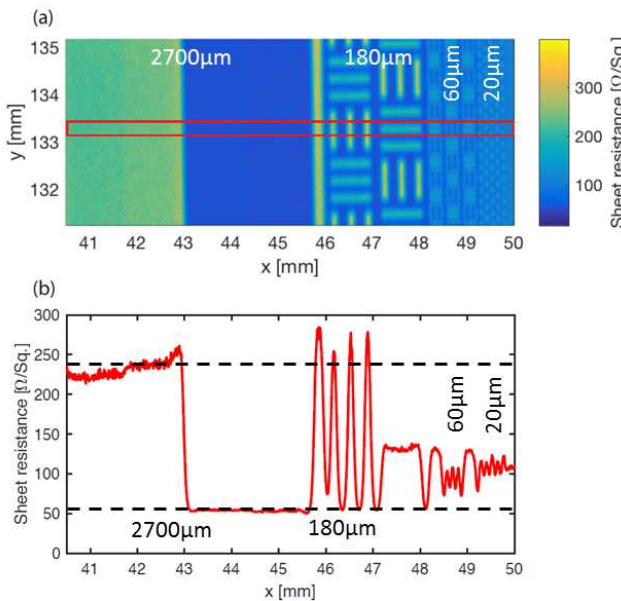


Fig 4. (a) R_{sheet} map of an area of the test structure sample. (b) R_{sh} values measured along one direction on the test structure (average of 10 lines). The area relative to this plot is shown by a red box in (a). The dashed lines in (b) are the known reference R_{sh} values.

Figure 4 shows a R_{sheet} map of part of the test structure (a) including several feature sizes (2700, 180, 60 and 20 μm), and a line scan of the same data taken along the x-axis direction (panel b, average of 10 lines). The dashed lines in Fig. 4(b) represent the known reference values of the features. As can be seen, the THz transmission method reliably reproduces the correct R_{sheet} values for feature sizes larger than 180 μm . For smaller feature sizes, while a R_{sheet} contrast is measured, the absolute values of R_{sheet} deviate from the real ones. In particular, a lower R_{sheet} contrast is observed and the resulting signal is a convolution of the real R_{sheet} pattern and the THz beam shape. We are currently working on using deconvolution techniques to improve the accuracy of R_{sheet} determination even feature size smaller than 180 μm .

III. DIELECTRIC OPENING OPTIMIZATION WITH THZ

A. Method

Samples were prepared from chemically polished n-type CZ 6-inch wafers. After BBr diffusion, a 70-nm-thick SiN_x layer was applied on both sides of the wafer by PECVD. A SmartEtch3000 paste (Merck) was screen printed on the wafer rear side using a screen with 1 mm wide busbars and 100 μm wide fingers. The etch paste was then cured at different temperatures in a belt furnace, with fixed belt speed. The paste was finally removed in a $\text{KOH}/\text{H}_2\text{O}_2$ bath heated at 60°C.

The samples were first studied by optical microscopy. Based on the color of the opened area, it is possible to judge whether a residual layer is present, if this layer is thicker than 30 nm

(see SiN_x color charts, [5]). However, it is not possible to observe if the diffusion layer has been altered. THz probing offers the unique opportunity to inspect the diffusion layer in the opening and thus to optimize the opening process.

B. Results

Polished samples with etch paste cured at different temperatures were studied with both optical microscopy and THz mapping. Figure 5 shows the effect of the paste curing temperature on the opening of the SiN_x , by means of microscope images of single fingers (top row), and R_{sheet} maps of the diffusion layer obtained with THz scanning (bottom row). The color scale of the THz maps refers to the R_{sheet} of the doped layer and is the same for the three plots. Three temperature are shown, corresponding to a reference temperature (T_{ref}), and to +30°C and +150°C temperature difference with respect to T_{ref} .

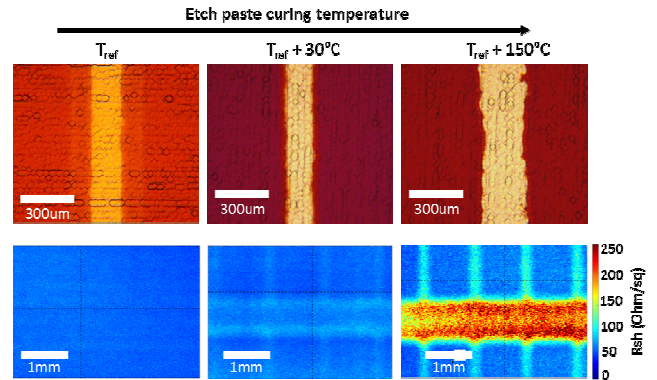


Fig 5. Microscope images (top row) and THz R_{sheet} maps (bottom row) of samples after SiN_x opening with etch paste, for 3 different curing temperatures.

For T_{ref} (left) the optical microscope clearly shows that the SiN_x has been etched, but is not fully opened (orange color in the opening). The THz R_{sheet} scan shows a homogeneous map of the sample with a constant R_{sheet} value of about 60 Ohm/sq. This is expected for a sample where the SiN_x is not fully opened, because there is no damage to the diffusion. Importantly, the map also shows that the THz method is not influenced by the morphology of the SiN_x layer, i.e. the THz mapping method does not show a “false contrast” due to changes in the SiN_x thickness. For a curing temperature of $T_{\text{ref}}+30^\circ\text{C}$ (center) and $T_{\text{ref}}+150^\circ\text{C}$ (right) the microscope shows deeper etching of the SiN_x . The THz R_{sheet} map shows a pattern of higher R_{sheet} in the region corresponding to the opened busbar and finger areas. The R_{sheet} in these areas increases up to a value of 90 Ohm/sq for the $T_{\text{ref}}+30^\circ\text{C}$, and up to 250 Ohm/sq for the highest temperature, as measured on the busbar area. The increase of R_{sheet} is attributed to partial etching of the diffused layer by the SmartEtch paste.

From this study we are thus able to optimize the curing temperature of the etch paste in order to avoid (or minimize)

the damage created by the etch paste to the diffusion. Using THz allows for optimization using half-fabricates of solar cells, while so far the optimization had to be conducted on fully functional cells which was usually more costly and time consuming.

IV. IBC CELLS WITH NFT PASTE

The optimization presented in the previous section was used as a starting point to make Mercury IBC solar cells with a NFT paste. The cells were made on 6-inch wafers with chemically polished rear side, following our standard process flow for Mercury cells [1]. The rear side was passivated with a $\text{Al}_2\text{O}_3/\text{SiN}_x$ layer stack. The opening of this dielectric stack was performed by combining the SmartEtch paste with a 1% HF dip. The aim was to partially open the rear side dielectric with the SmartEtch paste, and to complete the opening with the HF dip, without etching the exposed diffusions. A full optimization of the paste curing temperature and HF dip time was performed at cell level. The curing temperature was chosen between $T_{\text{ref}}+10^\circ\text{C}$ and $T_{\text{ref}}+70^\circ\text{C}$, i.e. around the optimal temperature found in the optimization study with THz. The HF dip time was varied between 2.5 and 10 minutes. In each case, the thickness of the front side SiN_x anti-reflection coating was corrected according to the HF dip time. The NFT paste was finally printed to contact the IBC cells, which were then measured in house in a Wacom solar simulator.

attributed to a non-complete opening of the dielectric stack before the application of the NFT metallization. The FF improves both by increasing the curing temperature and/or by increasing the HF dip time, due to a more effective opening of the dielectric. Overall, the first method seems to be more effective. The optimal FF value (from the fit) is obtained for $\Delta T=55^\circ\text{C}$ and the shortest HF time of 2.5 min. The lower FF values (relative to the optimum) observed for longer HF times, are related to losses in pseudo-FF (not shown), which could be attributed to a worsening of the passivation properties of the dielectric stack. It is known that a bad surface passivation at the rear side of IBC cells can cause pseudo-FF losses due to increased j_{02} recombination of the meandering pn-junction [6]. The best measured FF was 77.9%, obtained for cells with $\Delta T=40^\circ\text{C}$ and HF time = 2.5 min.

Figure 7 shows the cell V_{oc} surface response with respect to HF dip time and ΔT , similarly to what shown in Fig. 6 for the FF. A clear optimum value of V_{oc} is observed for relatively low curing temperature ($\Delta T=20^\circ\text{C}$) and for the shortest HF time. The best measured V_{oc} in this conditions was 654 mV. Note that this value is limited by a high j_0 of the passivated rear emitter surface ($j_{0,\text{emit}} > 100 \text{ fA/cm}^2$) relative to our standard baseline process ($j_{0,\text{emit}} = 45 \text{ fA/cm}^2$), as measured on symmetrical test structures. We are currently investigating the reasons for the worse surface passivation with respect to our baseline process.

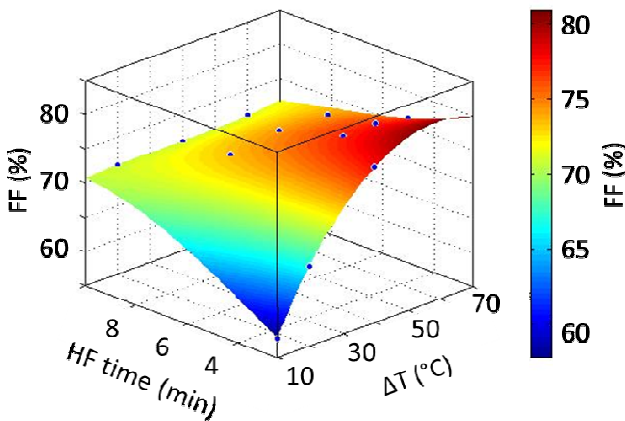


Fig 6. FF of IBC cells as a function of HF dip time (x-axis) and paste curing temperature (y-axis)

Figure 6 shows the fill-factor (FF) of the IBC cells (z-axis and color bar) as a function of the HF dip time (x-axis) and the temperature difference with respect to T_{ref} (ΔT , y-axis). The dots in the graph represent the measured values (each is an average of 3-5 cells). The color surface is a polynomial cubic fit of the measured data. Some clear trends are observed from the plot. First, a very low fill factor is observed for the lowest temperature in combination of the short HF dip. This is

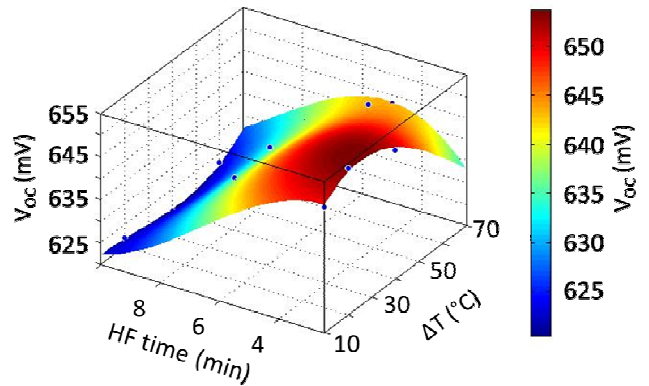


Fig 7. V_{oc} of IBC cells as a function of HF dip time (x-axis) and paste curing temperature (y-axis)

As can be seen from the graph, the dominant effect on the V_{oc} the HF dip time. A severe V_{oc} loss is observed for longer HF times, which is attributed to a worsening of the surface passivation due to etching of the dielectric stack. A reduction in V_{oc} is also noted for the highest curing temperatures ($\Delta T=70^\circ\text{C}$). This is attributed to damage of the diffusion layer below the contact due to over-etching of the SmartEtch paste.

In order to confirm this, Fig. 8 shows the R_{sheet} map of an unmetallized sample, obtained with a THz scan. The map shows several R_{sheet} contrasts. The main modulation is between

the BSF and emitter fingers, which have resistivities of ~ 20 Ohm/sq (blue) and 90 Ohm/sq (green, used as reference area), respectively. At the center of the emitter finger, a clear area with much higher R_{sheet} (~ 200 Ohm/sq, red) is visible, corresponding to the area opened by the SmartEtch paste. A higher R_{sheet} in this area causes a less effective “shielding” of minority carriers from the metal contact and thus larger contact recombination. Interestingly, the R_{sheet} map also reveals a sub-pattern in the opening area, where periodic blobs of higher R_{sheet} (i.e. deeper etch) are visible along the finger direction, corresponding to the mesh of the screen used for printing the SmartEtch paste. This feature reveals the etching dynamic of the etch paste, and it could only be detected using the high-resolution THz mapping method.

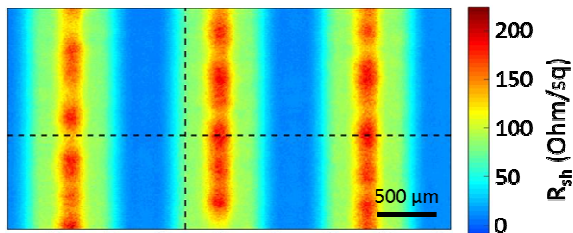


Fig 8. R_{sheet} map of an IBC structure, revealing the etching dynamics of the screen printed paste.

Overall, the best cell was obtained with a curing temperature of $T_{ref}+50^{\circ}\text{C}$, combined with an HF dip of 2.5 min. The best measured cell efficiency was 20.8%. The table below reports the IV parameters of the best cell, as measured in-house without spectral mismatch correction.

Best cell IV parameters	
J_{sc} (mA/cm ²)	41.1
V_{oc} (mV)	649.2
FF (%)	77.7
Efficiency (%)	20.8

V. CONCLUSION

We have presented a new method to optimize the SiN_x opening of IBC solar cells for application of NFT paste. This method is based on THz transmission measurements and allows to study diffusion layers with resolutions down to 20 μm . This method is also applicable to solar cell half-fabricates, thus avoiding the processing of full cell for parameter optimization. We have presented a preliminary study on the accuracy of R_{sheet} determination with the THz transmission method, and concluded that absolute R_{sheet} values can be measured for features down to 180 μm . For smaller features a reduction in the R_{sh} contrast is observed. As an example of the THz capabilities, we have studied the case of opening of a dielectric layer stack with an etching paste, prior to the application of a NFT metallization. In our study, we optimize the curing temperature of the etch paste in order to avoid damage to the diffusion layer. We used THz R_{sheet} mapping to identify the range of curing temperatures most suited for the opening process. A full optimization of this latter was performed on cell level. The results have been presented, with cell efficiencies up to 20.8%.

REFERENCES

- [1] I. Cesar, et al. “Enablers for integral IBC cell and module development and implementation in PV industry”, 26th PVSEC (2016)
- [2] A. Mewe, et al. “Emitter and contact optimization for high efficiency IBC Mercury cells”, 31st EUPVSEC (2016)
- [3] A. Cuevas, et al. “Surface recombination velocity of highly doped n-type silicon”, J. of Appl. Phys. 80 (6), 3370-3375 (1996)
- [4] M. Nagel, et al. “THz microprobe system for contact-free high-resolution sheet resistance imaging,” 28th EUPVSEC (2013)
- [5] http://www.cleanroom.byu.edu/color_chart.phtml
- [6] P. Spinelli, et. al. “Quantification of PN-junction Recombination in IBC Crystalline Silicon Solar Cells”, in press, IEEE Journal of Photovoltaics (2017)